

# Analysis of the measurement of polarization-shaped ultrashort laser pulses by tomographic ultrafast retrieval of transverse light $E$ fields

Lina Xu,<sup>1,\*</sup> Philip Schlup,<sup>2</sup> Omid Masihzadeh,<sup>2</sup> Randy A. Bartels,<sup>2</sup> and Rick Trebino<sup>1</sup>

<sup>1</sup>School of Physics, Georgia Institute of Technology, Atlanta, Georgia 30332, USA

<sup>2</sup>Department of Electrical and Computer Engineering, Colorado State University, Fort Collins, Colorado 80523, USA

\*Corresponding author: gth665y@mail.gatech.edu

Received June 10, 2009; accepted July 12, 2009;  
posted October 12, 2009 (Doc. ID 111992); published November 18, 2009

We consider in detail the technique of tomographic ultrafast retrieval of transverse light  $E$  fields (TURTLE) for measuring the evolution of an arbitrary, potentially complex, and ultrashort laser pulse's intensity-and-phase and polarization-state evolutions in time. TURTLE involves making three ultrashort-pulse measurements using established single-polarization pulse-measurement techniques. Two of the measurements are of the pulse's orthogonal linear polarizations (e.g., horizontal and vertical) and the third occurs for an arbitrary additional polarization angle (e.g., 45°). If the field projections are measured using second-harmonic-generation frequency-resolved optical gating, we demonstrate that a simple optimization can accurately and reliably retrieve the time-dependent polarization state, even for very complex polarization-shaped pulses. © 2009 Optical Society of America

OCIS codes: 260.5430, 320.5540, 260.7120.

## 1. INTRODUCTION

Polarization-varying complex ultrashort laser pulses were first used in quantum control [1–5] and are now playing roles in many areas of research. Such “polarization-shaped” pulses have been considered for the generation and measurement of high-harmonic pulses [6] and for the control of two-dimensional lattice vibrations in crystals [7]. Polarization-shaped pulses have been generated by various means, mostly based on Fourier-domain pulse shaping of individual polarization components [3,8–11]. On the other hand, only a few methods exist to measure them. Time-resolved ellipsometry (TRE) [12,13] was one of the first technologies used to characterize the polarization evolution of ultrashort pulses. It involves measuring all four Stokes parameters of the pulse, but it is labor intensive. A simpler technique is polarization-labeled interference versus wavelength for only a glint (POLLIWOG) [14], which uses spectral interferometry [15] to characterize—successively or simultaneously—the two orthogonal polarization components relative to a well-characterized reference pulse. Other approaches involve measuring the spectrum and the cross correlation of the polarization components or the cross-phase modulation, both combined with iterative numerical algorithms [16,17]. POLLIWOG is the most commonly used technique, and it works well; but it requires careful phase stabilization and measurement of the relative phase between the two polarizations, and it requires a separate self-referenced technique for measuring the required reference pulse.

Recently, we introduced a self-referenced technique for

measuring polarization-shaped pulses, which we called tomographic ultrafast retrieval of transverse light  $E$  fields (TURTLE) (Fig. 1) [18]. It does not require a separate well-characterized reference pulse and is based on measuring the electric field versus time at three different linear polarizations, obtained by making such measurements after a polarizer for three different polarizer angles. Two of the measurements characterize the electric field for mutually orthogonal field components, and the third—measured at an arbitrary angle in between (typically 45°)—is used to determine the phase relationship between these components, which yields the full vector polarization evolution of the pulse. Any established method that determines the complex field  $\tilde{E}(\Omega)$  of a single linear polarization can, in principle, be used in TURTLE. In addition the pulse energy or the average power must be measured for each polarization. No modifications to the standard pulse-measurement apparatus are needed.

Here we study TURTLE technique using second-harmonic-generation frequency-resolved optical gating (SHG FROG) by performing detailed simulations. We simulate TURTLE's performance using SHG FROG for simple and complex polarization-shaped pulses and find that it works very well, even for very complex pulses. Our simulations show that an error minimization algorithm using the SHG FROG trace performs robustly—even in the presence of added noise. We attribute this robust behavior to the well-known overdetermination of the pulse complex electric field afforded by a FROG trace.

We chose FROG because it is the most mature self-referenced pulse-measurement technique available and

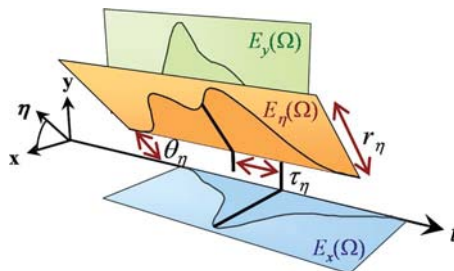


Fig. 1. (Color online) Schematic visualization of the TURTLE principle. The time-evolving electric field vector  $\mathbf{E}(t)$  (not shown) is characterized by measuring linear projections  $\tilde{E}_x(\Omega)$ ,  $\tilde{E}_y(\Omega)$ , and  $E_\eta(\Omega)$  in the frequency domain using an existing ultrashort-pulse characterization technique. The algorithm establishes the relative amplitude  $r$ , delay  $\tau$ , and phase  $\theta$  between the projections to retrieve the full vector field.

has been shown to measure accurately the full intensity and the phase of an arbitrary complex ultrashort pulse [19], subject only to trivial ambiguities. Specifically we chose SHG FROG due to its high sensitivity and prevalence. Also, it has minimal ambiguities and then only trivial ones. Trivial ambiguities of standard SHG FROG include the direction of time (DOT) of the pulse; that is, SHG FROG cannot distinguish between a reconstructed field  $\tilde{E}(\Omega)$  and its complex conjugate,  $\tilde{E}^*(\Omega)$ . For pulses that are well-separated in either optical frequency or time, an additional ambiguity arises in their relative phases  $\Delta\varphi$  [20,21]. For example, relative phases of both  $\Delta\varphi$  and  $\Delta\varphi + \pi$  yield the same SHG FROG trace for double pulses in time. However, it has been shown that these trivial ambiguities can easily be removed using simple techniques that involve minimal additional effort. Adding a known spectral dispersion (chirp) and performing a second FROG measurement removes the DOT ambiguity. Even better, replacing the FROG beam splitter with an etalon generates identical trains of overlapping (and decaying) pulses in both arms of the device; such waveforms do not experience such ambiguities, and the original pulse can be retrieved from them easily and unambiguously [22], except for the usual absolute-phase and arrival-time ambiguities common to all self-referenced pulse-measurement techniques. Thus FROG and its variations yield the best-posed (least ambiguous) set of self-referenced pulse-measurement techniques currently available.

While these remaining two ambiguities are generally considered trivial, and they are for most purposes, they are not so trivial for the measurement of polarization-shaped pulses. Nonmeasurement of the absolute phase and time preclude the determination of key quantities of the full vector field. Specifically, what distinguishes monochromatic 45° linear polarization from circular polarization is the relative phase of the horizontal and vertical polarizations, which is the difference between the two pulse absolute phases, which are not measured in self-referenced pulse-measurement techniques in general. And what distinguishes 45° linear polarization from two well-separated pulses of orthogonal polarization is, of course, their relative arrival times. Thus these two otherwise trivial ambiguities are not so trivial for polarization-shaped pulses and thus become the principal unknowns

that TURTLE aims to determine. It is the third FROG trace that accomplishes this. The only case we have found in which TURTLE, as described above, does not work is the trivial case in which the two polarization components are identical, and the polarization thus does not actually evolve, but this ambiguity can easily be removed with one additional measurement.

## 2. THEORY

In the frequency domain, we write the polarization-shaped vector field as

$$\tilde{\mathbf{E}}(\Omega) = \tilde{E}_x(\Omega)\hat{\mathbf{x}} + r\tilde{E}_y(\Omega)e^{-i(\Omega\tau+\theta)}\hat{\mathbf{y}}, \quad (1)$$

where the optical angular frequency  $\Omega \equiv \omega - \omega_0$ , and  $\tilde{E}_x(\Omega)$  and  $\tilde{E}_y(\Omega)$  represent the complex frequency-domain polarization components along the Cartesian axes, with the beam propagating along  $\hat{\mathbf{z}}$ . We use this formulation because ultrafast polarization shapers typically operate by independently shaping orthogonal polarization components. To obtain the full polarization information, we need to know not only the fields  $\tilde{E}_x(\Omega)$  and  $\tilde{E}_y(\Omega)$  but also the relative amplitude  $r$ , the relative delay  $\tau$ , and the relative phase  $\theta$  between the components. No existing self-referenced single-polarization pulse-measurement technique is able to provide absolute time or phase information, but it is easy to measure the relative amplitude using a simple energy detector as given below. The measurement technique that we call TURTLE determines these relative quantities from an additional SHG FROG trace of the polarization component, projected here at 45° between  $\hat{\mathbf{x}}$  and  $\hat{\mathbf{y}}$ . In the following, we label this projection angle  $\eta$ .

The easiest ambiguity to resolve is the relative amplitude ratio  $r$ . We can determine it experimentally by measuring the average power  $P$  for each linear projection measurement. The power can be written as

$$P \propto \int_{-\infty}^{\infty} |r'\tilde{E}(\Omega)|^2 d\Omega = r'^2 \int_{-\infty}^{\infty} |\tilde{E}(\Omega)|^2 d\Omega, \quad (2)$$

where  $r'$  is a scaling factor that relates the reconstructed arbitrarily normalized field  $\tilde{E}(\Omega)$  to the physically present field. So, if we normalize the retrieved fields according to  $\int |\tilde{E}(\Omega)|^2 d\Omega = 1$ , then we can find  $r$  in Eq. (1) from  $r = \sqrt{P_y/P_x}$ . As we show below, the power measurements are critical for the trivial case of pure elliptical polarization as shown below, where the reconstructed fields are identical except for the amplitude factors. In the following simulations, we set  $r=1$  without loss of generality.

TURTLE aims to determine the relative delay  $\tau$  and the relative phase  $\theta$  in Eq. (1) using an additional polarization projection at angle  $\eta$ . We denote this projected field as  $\tilde{E}_\eta(\Omega)$ , and it can be written as

$$\tilde{E}_\eta(\Omega) = \cos \eta \tilde{E}_x(\Omega) + r \sin \eta \tilde{E}_y(\Omega) e^{-i(\Omega\tau+\theta)}. \quad (3)$$

A choice of  $\eta=45^\circ$  will usually give the best results because  $\tilde{E}_x(\Omega)$  and  $\tilde{E}_y(\Omega)$  contribute equally to the projected field  $\tilde{E}_\eta(\Omega)$ . We choose this angle in the simulations below.

The expression for the SHG FROG trace of a single linearly polarized pulse temporal electric field  $E(t)$  is [23]

$$I_{\text{FROG}}(\omega, T) = \left| \int_{-\infty}^{\infty} E(t)E(t-T)e^{-i\omega t} dt \right|^2. \quad (4)$$

The FROG trace is collected by recording the second-harmonic spectra generated as the delay  $T$  between two replicas of  $E(t)$  is varied. From the SHG FROG trace, an established generalized-projections algorithm reliably finds the full intensity and phase of an arbitrary ultrashort laser pulse [23]. Thus,  $\tilde{E}_x(\Omega)$  and  $\tilde{E}_y(\Omega)$  can readily be determined experimentally without the need for additional reference pulses.

Having found  $\tilde{E}_x(\Omega)$  and  $\tilde{E}_y(\Omega)$ , we use a minimization algorithm to find the relative delay  $\tau$  and the relative phase  $\theta$  for which  $\tilde{E}_x(\Omega)$  and  $\tilde{E}_y(\Omega)$  yield the projected field  $\tilde{E}_\eta(\Omega)$ . The algorithm can find these parameters using the additional information contained in the  $\eta$ -projected SHG FROG trace. We sample the FROG traces onto regularly spaced optical frequency  $\omega_i$  and delay  $T_j$  axes in an  $N \times N$  grid. We calculate the projected FROG trace from  $\tilde{E}_\eta(\Omega)$  using Eq. (4), and TURTLE involves minimizing the difference between the calculated  $I_\eta^{\text{calc}}(i, j)$  and the measured  $I_\eta^{\text{meas}}(i, j)$  traces. We use the criterion of the RMS error defined as [24]

$$e = \frac{\sqrt{\sum_{i,j=1}^N [I_\eta^{\text{meas}}(i,j) - I_\eta^{\text{calc}}(i,j)]^2}}{\sqrt{\sum_{i,j=1}^N [I_\eta^{\text{meas}}(i,j)]^2}}, \quad (5)$$

which describes the difference between the two FROG traces  $I_\eta^{\text{meas}}$  and  $I_\eta^{\text{calc}}$  divided by the nonzero area. The error  $e$  is then minimized with respect to the iterated values of  $\tau$  and  $\theta$ , with the optimal values corresponding to those values of  $\tau$  and  $\theta$  that minimize  $e$ . In the simulations, we calculate the error surface  $e(\tau, \theta)$  about the optimal values.

We must also ensure that TURTLE uses the correct *relative* DOT between the components  $\tilde{E}_{x,y}(\Omega)$ , since a wrong DOT in one projection and the correct DOT in the other no longer corresponds to the vector field being measured. This ambiguity is easily resolved in two ways: we can determine the overall correct DOT for both fields,  $\tilde{E}_x(\Omega)$  and  $\tilde{E}_y(\Omega)$ , by placing an etalon or adding a known amount of material chirp in one of more of the SHG FROG measurements. This is the standard method for resolving the time ambiguity in SHG FROG. In TURTLE, knowing the DOT of one component,  $\tilde{E}_x(\Omega)$  or  $\tilde{E}_y(\Omega)$ , is sufficient to determine that of the other and hence that of the entire polarization-shaped pulse. In other words, if only the shape of the vector field—but not its absolute DOT—is needed, we can calculate the error  $e(\tau, \theta)$  separately for both combinations of relative DOTs:  $\tilde{E}_x(\Omega) + \tilde{E}_y(\Omega)$  and  $\tilde{E}_x(\Omega) + \tilde{E}_y^*(\Omega)$ . The TURTLE trace for non-trivial vector pulse shapes is sensitive to the relative DOT, so the minimum error in  $e$  will be lower for the correct relative DOT.

To simulate the practical environment, we added 0.5% Poisson noise to each SHG FROG trace. In this approach, the measured trace with such an additive noise [23] at each pixel is

$$I_{\text{FROG}}^{(\bar{\eta})}(\omega_i, \tau_j) = I_{\text{FROG}}(\omega_i, \tau_j) + \eta_{ij}\alpha/\bar{\eta}, \quad (6)$$

where  $\eta_{ij}$  is a pseudorandom number drawn from a Poisson distribution of mean  $\bar{\eta}$  and  $\alpha$  is the noise fraction. We verified that the maximum trace value at the edges of the array is less than 0.5% of the peak value of the FROG trace. Suppressing the background noise is important in SHG FROG measurements. Any nonzero average background (due to noise) in a FROG trace implies spurious nonzero intensity at large times and with high frequency in the pulse, that is, spurious pulse wings with high frequency noise. So, in practice, before running the pulse retrieval program, background subtraction is always performed. Several methods are available, and they include Fourier low-pass filtering, corner suppression, and mean-background subtraction. In our simulations, we chose to perform only simple mean-background subtraction (although performing the others as well would likely have further improved the performance beyond what we observe). The mean of the noise was obtained by averaging the values in the  $5 \times 5$  pixel squares in the four corners of the FROG trace (i.e., far from the center of the trace, where the most important pulse information is located). After subtracting this constant background from all points in the trace, we set all the resulting negative points to zero (as is usually done).

We found the values of the relative phase and delay using the 45° polarized FROG trace and the fields determined from the  $x$ - and  $y$ -polarized traces, using a MATLAB simplex minimization routine for multidimensional unconstrained optimization [25]. This routine is ideal for the TURTLE technique because, while simplex routines are known to be slow, TURTLE involves only a two-parameter minimization, and so it converges relatively quickly (typically 1 min or so for a  $256 \times 256$  trace on a laptop). Also, simplex routines are less likely than derivative-based routines to fall into possible local minima.

### 3. SIMULATIONS

Below we give several examples of using the TURTLE technique to find the polarization state of an ultrashort pulse. While the majority of TURTLE measurements are anticipated to be used to characterize complex pulses with complex polarization evolution, we begin with some simple cases since the extremely simple case of nonevolving polarization with identical  $x$  and  $y$  components revealed the only ambiguity we encountered in our study. The ambiguity disappears in the presence of even slight polarization complexity and so is unlikely to present problems for the use of TURTLE.

The first example pulse comprises two identical  $\hat{x}$  and  $\hat{y}$  components consisting of transform-limited Gaussian pulses with a full width at half-maximum (FWHM) duration of 30 fs so that  $E_x(t) = \exp\{-2 \ln 2[t/30 \text{ fs}]^2\}$  and  $E_y(t) = \exp\{-2 \ln 2[(t+\tau/2)/30 \text{ fs}]^2\}$ . The relative delay and

the relative phase between the polarization components were  $\tau=170$  fs and  $\theta=\pi/3$ . The resulting SHG FROG traces for the projected fields  $\tilde{E}_x(\Omega)$ ,  $\tilde{E}_y(\Omega)$ , and  $\tilde{E}_\eta(\Omega)$  are shown in Figs. 2(a)–2(c), respectively. In Figs. 2(d) and 2(e), we show the pulse intensity and the temporal phase reconstructed from the SHG FROG traces for  $E_x(t)$  and  $E_y(t)$ . The peak intensity is set at  $t=0$ . The zero order and first order spectral phases, which correspond to the relative phase and delay in the evolution of the polarization, are not reflected in these two retrieved fields. The relative phase and delay are obtained from the SHG FROG trace of  $\tilde{E}_\eta(\Omega)$ . Since the pulses are symmetrical in time and frequency, the reconstructed field projections closely match the generating fields, in particular with regard to the absolute time and phase of each component.

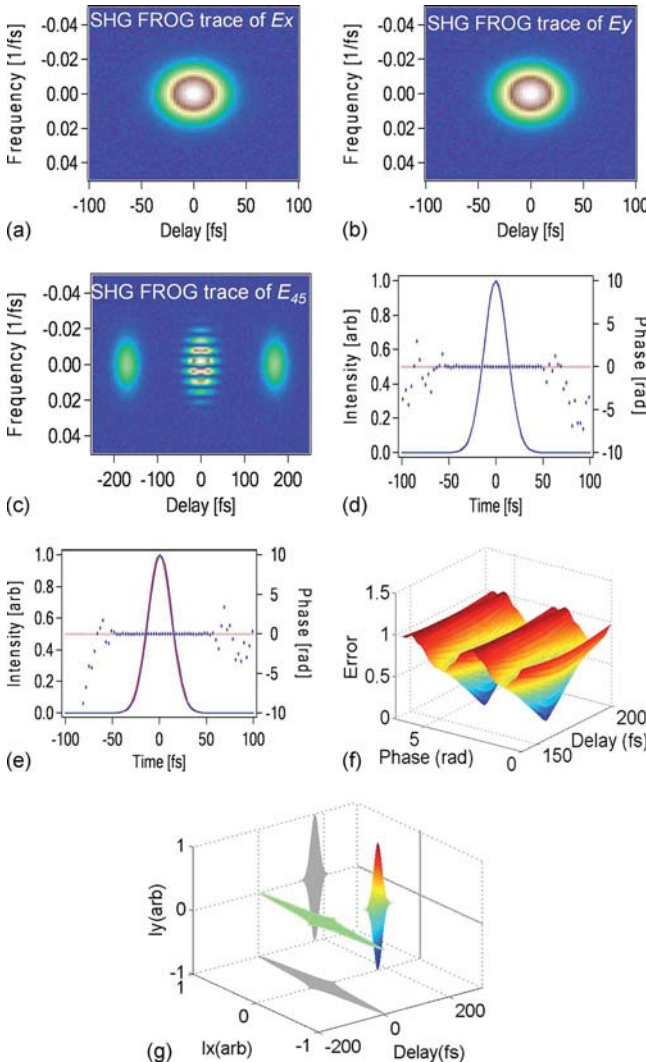


Fig. 2. (Color online) TURTLE retrieval steps for a vector field consisting of two transform-limited Gaussian components separated by  $\tau=170$  fs. (a),(b),(c) Simulations of measured SHG FROG traces for  $\tilde{E}_x(\Omega)$ ,  $\tilde{E}_y(\Omega)$ , and  $\tilde{E}_\eta(\Omega)$ , respectively, with  $\eta=45^\circ$ . (d),(e) Pulse fields  $E_x(t)$ ,  $E_y(t)$  obtained using the standard reconstruction algorithm (dots), compared with the generating fields (solid curve). (f) The error surface; the two minima indicate the  $\pi$  rad phase ambiguity arising from the SHG FROG trace of two pulses well separated in time. (g) Sketch of the full vector field  $E(t)$ .

Figure 2(f) shows the error surface  $e$ , about the target values of  $\tau$  and  $\theta$ , calculated using the reconstructed  $\tilde{E}_{x,y}(\Omega)$  and the  $\eta$ -projected FROG trace  $I_\eta$  from Eq. (5). On this error surface, the parameter minimization retrieved a relative delay of 169.65 fs and a relative phase of  $0.3344\pi$  or  $1.3316\pi$  rad, depending on the initial guess. This is the expected  $\pi$  rad phase ambiguity that arises from SHG FROG traces for pulses separated in time; as discussed above, an additional measurement by adding additional chirp on either one of the pulses or both pulses to make  $E_x(t)$  and  $E_y(t)$  overlap in time can be used to eliminate this ambiguity. A three-dimensional representation of the vector field  $E(t)$  is sketched in Fig. 2(g). Examination of the  $\eta$ -projected SHG FROG trace of Fig. 2(c) reveals spectral intensity modulations at a FROG delay of  $T=0$ . As discussed in Section 2, these fringes correspond to spectral interferometry fringes, and their spacing is inversely proportional to  $\tau$ , and the peak locations relative to  $\Omega=0$  are given by  $\theta$ .

Combining the identical fields  $\tilde{E}_x(\Omega)$  and  $\tilde{E}_y(\Omega)$  from the previous example with  $\tau=0$  and  $\theta=\pm\pi/2$  yields a circularly polarized pulse shown in Fig. 3. In this case, we can relate the field components by  $\tilde{E}_y(\Omega)=\tilde{E}_x(\Omega)e^{-i\theta}$  so that the  $\eta$ -projected SHG FROG trace for  $\eta=45^\circ$  will be given by

$$I_{\text{FROG}}(\omega, T) = |(1 + e^{i\theta})^2|^2 \int E_x(t) E_x(t - T) e^{-i\omega T} dt^2.$$

Thus, the projections  $\hat{x}$  and  $\hat{y}$  yield identical SHG FROG traces [Fig. 3(a)] with the  $\eta$  projection being qualitatively the same but scaled by an intensity-weighting factor of  $|(1 + e^{-i\theta})^2|^2 = [2(1 + \cos \theta)]^2$ . Since this factor does not depend on the sign of  $\theta$ , which determines the handedness of the vector field, TURTLE cannot distinguish between left and right circularly polarized fields. This can be seen in the error surface shown in Fig. 3(b), which indicates two symmetric minima at  $\pm\theta$ . The TURTLE fitting algorithm retrieved a relative delay of  $\tau=0.0174$  fs and a relative phase of  $\theta=0.5014\pi$  or  $-0.5015\pi$  rad, depending on the initial guess. Further, in this case of indistinguishable SHG FROG traces, the normalization of Eq. (5) and that inherent in the standard FROG reconstruction algorithm means that the ellipticity, determined by the relative amplitude  $r$  of the  $\hat{x}$  and  $\hat{y}$  components, cannot be directly determined. An independent power or pulse energy measurement is thus necessary to determine the ellipticity.

The handedness ambiguity can be resolved by introducing different chirps to the two components as shown in Fig. 4. Here, we added  $\varphi^{(2)}(\Omega)=\pm 200$  fs<sup>2</sup>/rad quadratic spectral phase to each of  $\tilde{E}_{x,y}(\Omega)$ . The SHG FROG traces for these components are still indistinguishable [Fig. 4(a)] but, due to the knowledge of the signs of the added chirps, we can correctly reconstruct the fields as shown in Figs. 4(b) and 4(c). The  $\eta$ -projected SHG FROG trace, shown in Fig. 4(d), is now distinct and its shape uniquely determines the correct phase since the error surface [Fig. 4(e)] exhibits only a single minimum. The retrieved relative delay and phase were  $\tau=-1.0242$  fs and  $\theta=0.5183\pi$  rad, identifying the pulse as right circularly polarized. Alternatively, we could characterize the pulses transmitted

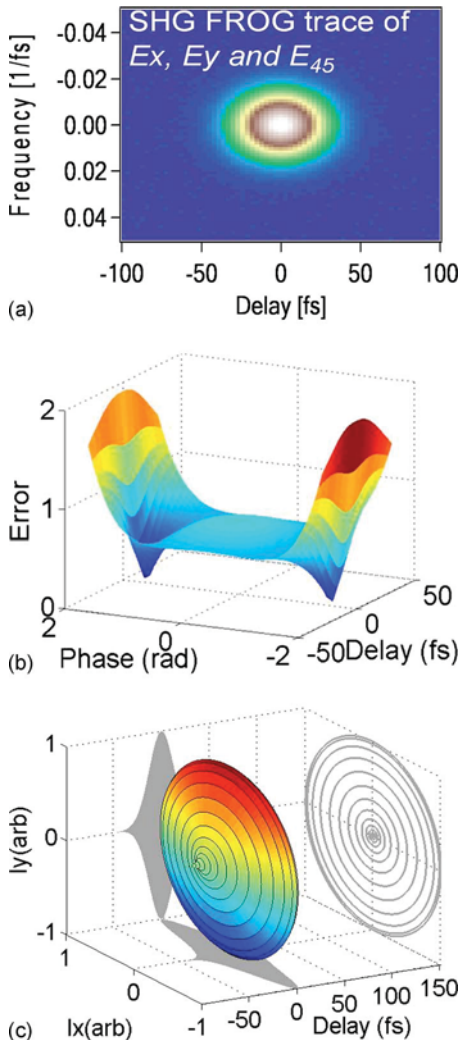


Fig. 3. (Color online) (a) Simulation of measured SHG FROG traces; in this case all three projections yield the same trace. (b) The error surface; the two minima indicate an ambiguity in the chirality of the vector field  $\mathbf{E}(t)$ , which is shown in (c).

through a circular polarizer, analogously to the determination of one of the four Stokes vectors needed to fully define the vector field. The ambiguity in the sign of  $\theta$  arises only in the case of transform-limited temporally symmetric pulses and is not expected to occur for polarization-shaped pulses.

We show in Fig. 5 results from a randomly generated more complex pulse. We simulate an arbitrary vector field  $\mathbf{E}(t)$  by creating random complex field components for  $\tilde{E}_x(\Omega)$  and  $\tilde{E}_y(\Omega)$  and by applying Gaussian amplitude filters in both time and frequency domains. For the pulse shown in Fig. 5, the temporal and frequency filter FWHM widths were  $\Delta t = 180$  fs and  $\Delta\Omega = 0.3$  rad/fs. The resulting time-bandwidth products (TBPs) were 17.8 for the  $\hat{x}$ - and 13.0 for the  $\hat{y}$ -polarized components. We chose relative delay and phase values of  $\tau = 60$  fs and  $\theta = \pi/3$  rad, respectively. The SHG FROG traces of Figs. 5(a)–5(c) show a rapid structure characteristic of nontrivial pulses. As shown in Figs. 5(d) and 5(e), we verified that the FROG reconstructions were in good agreement with the generating fields, and from the error surface [Fig. 5(f)] the mini-

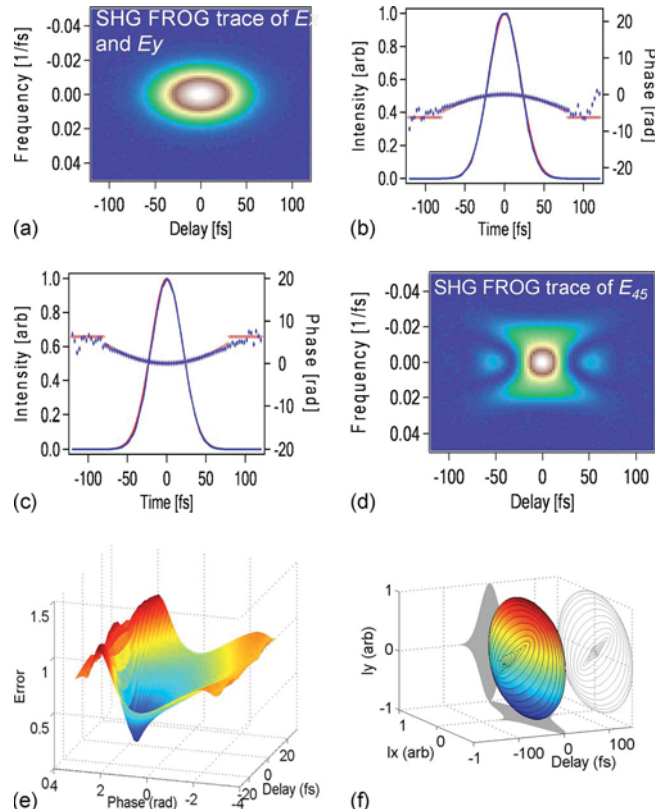


Fig. 4. (Color online) Establishing the chirality of a circularly polarized field by adding a known chirp; cf. Fig. 3. (a) Simulation of measured SHG FROG trace for  $\tilde{E}_x(\Omega)$ ; an identical trace is recorded for  $\tilde{E}_y(\Omega)$ . (b),(c) Pulse fields  $E_x(t), E_y(t)$  obtained using the standard reconstruction algorithm (dots), compared with the generating fields (solid curve). (d) SHG FROG trace for the  $\eta$ -projected component. (e) The error surface that shows only a single minimum at  $\theta = +\pi/2$ . (f) Sketch of the full vector field  $\mathbf{E}(t)$ .

mization algorithm retrieved relative delay and phase values of 62.74 fs and  $0.3349\pi$  rad, respectively.

Another case with a more complex pulse is shown in Fig. 6. The method to generate these two complex pulses is the same as the previous case. The temporal and frequency filter FWHM widths in this case were  $\Delta t = 1800$  fs and  $\Delta\Omega = 0.3$  rad/fs. The resulting TBPs were 169.7 for the  $\hat{x}$ - and 180.4 for the  $\hat{y}$ -polarized components. Due to the limitation of the computer memory, these are the most complicated pulses generated. We chose relative delay and phase values of  $\tau = 500$  fs and  $\theta = \pi/3$  rad, respectively. The SHG FROG traces of Figs. 6(a)–6(c) show a rapid structure characteristic of highly nontrivial pulses. As shown in Figs. 6(d) and 6(e), we verified that the FROG reconstructions were in good agreement with the generating fields, and from the error surface [Fig. 6(f)] the minimization algorithm retrieved relative delay and phase values of 504.96 fs and  $0.35\pi$  rad, respectively.

Table 1 shows some cases with different pulse complexities. All these  $x$  and  $y$  components are generated from random pulses filtered by a clean Gaussian pulse with FWHM widths of  $\Delta t = 900$  fs in the time domain and  $\Delta\Omega = 0.3$  rad/fs in the frequency domain. We chose relative delay and phase values of  $\tau = 500$  fs and  $\theta = 0.33\pi$  rad, respectively, for all cases. Without any noise added, the exactly correct relative delay and relative

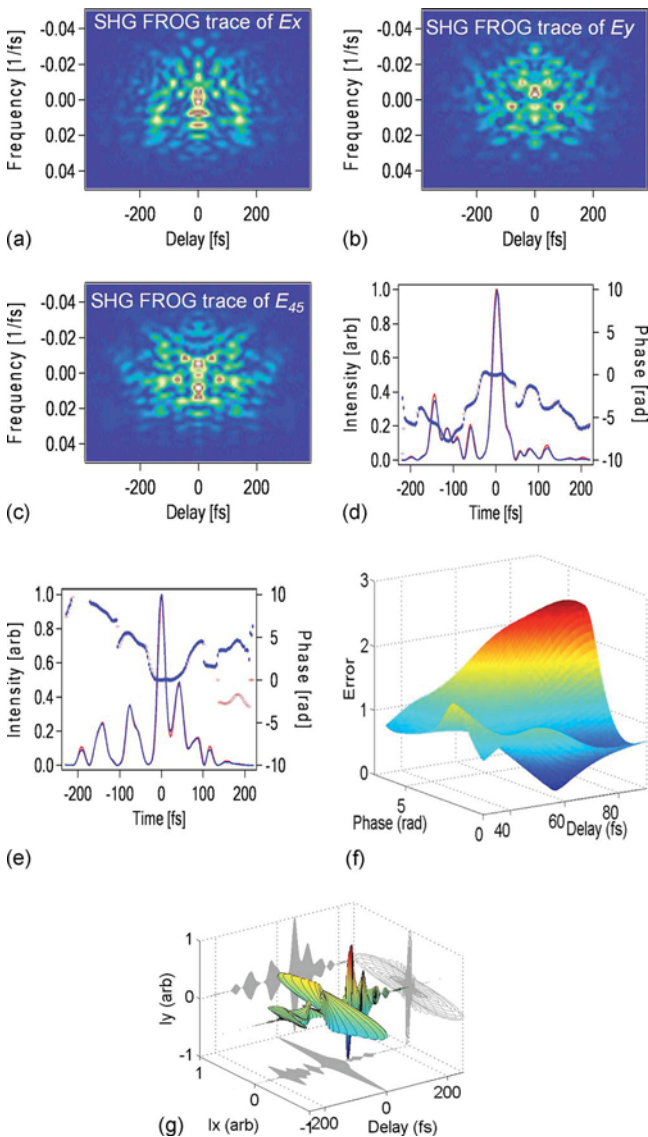


Fig. 5. (Color online) TURTLE retrieval steps for a randomly generated vector field. (a),(b),(c) Simulations of measured SHG FROG traces for  $\tilde{E}_x(\Omega)$ ,  $\tilde{E}_y(\Omega)$ , and  $\tilde{E}_\eta(\Omega)$ , respectively. (d),(e) Pulse fields  $E_x(t)$ ,  $E_y(t)$  obtained using the standard reconstruction algorithm (dots), compared with the generating fields (solid curve). (f) The error surface and (g) sketch of the full vector field  $\mathbf{E}(t)$ .

phase can be reconstructed in each case. With 0.5% Poisson noise added, the retrieved values are varied by at most 1.3% in the relative delay and 7.5% in the relative phase.

#### 4. CONCLUSIONS

We have analyzed the performance of TURTLE using SHG FROG for the self-referenced measurement of the complete vector field intensity and phase of polarization-shaped ultrashort laser pulses. Our simulations show that TURTLE works very well, robustly yielding the complete vector polarization even of very complex pulses and in the presence of noise. Indeed, the SHG FROG TURTLE minimization also reliably distinguishes the relative DOTs of the polarizations. We found no nontrivial ambi-

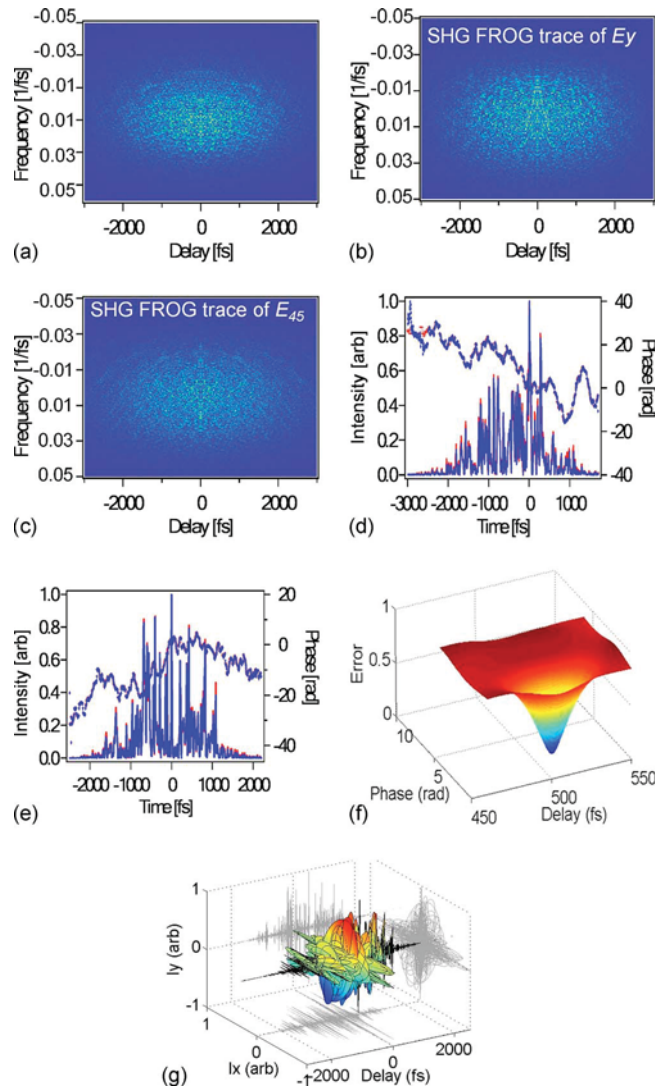


Fig. 6. (Color online) TURTLE retrieval steps for a randomly generated very complex vector field. (a),(b),(c) Simulations of measured SHG FROG traces for  $\tilde{E}_x(\Omega)$ ,  $\tilde{E}_y(\Omega)$ , and  $\tilde{E}_\eta(\Omega)$ , respectively. (d),(e) Pulse fields  $E_x(t)$ ,  $E_y(t)$  obtained using the standard reconstruction algorithm (dots), compared with the generating fields (solid curve). (f) The error surface and (g) sketch of the full vector field  $\mathbf{E}(t)$ .

guities. We expect this success to extend to TURTLE based on other FROG nonlinearities. We conclude that SHG-FROG-based TURTLE is a reliable technique for

**Table 1. Different Pulses with Their Reconstructed Relative Delays And Relative Phases**

TBP (x component)	TBP (y component)	Reconstructed $\tau$	Reconstructed $\theta$
84	121.8	501.23	$0.329\pi$
103.3	95	493.65	$0.359\pi$
57.7	89.5	501.59	$0.325\pi$
70.5	37.5	497.52	$0.329\pi$
100.4	79.2	499.54	$0.333\pi$
83.2	110.7	504	$0.318\pi$

self-referenced measurements of polarization states of even very complex polarization-shaped pulses.

## ACKNOWLEDGMENTS

The authors at the Georgia Institute of Technology acknowledge the Georgia Research Alliance for financial support. The portion of this work performed at Colorado State University (CSU) was partially supported by the Monfort Family Foundation and National Science Foundation (NSF) ECCS-0348068.

## REFERENCES

- W. S. Warren, H. Rabitz, and M. Dahleh, "Coherent control of quantum dynamics: the dream is alive," *Science* **259**, 1581–1589 (1993).
- T. Brixner, G. Krampert, T. Pfeifer, R. Selle, G. Gerber, M. Wollenhaupt, O. Graefe, C. Horn, D. Liese, and T. Baumert, "Quantum control by ultrafast polarization shaping," *Phys. Rev. Lett.* **92**, 208301 (2004).
- T. Brixner, N. H. Damrauer, G. Krampert, P. Niklaus, and G. Gerber, "Adaptive shaping of femtosecond polarization profiles," *J. Opt. Soc. Am. B* **20**, 878–881 (2003).
- T. Suzuki, S. Minemoto, T. Kanai, and H. Sakai, "Optimal control of multiphoton ionization process in aligned I2 molecules with time-dependent polarization pulses," *Phys. Rev. Lett.* **92**, 133005 (2004).
- M. Kakehata, R. Ueda, H. Takada, K. Torizuka, and M. Obara, "Combination of high-intensity femtosecond laser pulses for generation of time-dependent polarization pulses and ionization of atomic gas," *Appl. Phys. B* **70**, s207–s213 (2000).
- E. Constant, V. D. Taranukhin, A. Stolow, and P. B. Corkum, "Methods for the measurement of the duration of high-harmonic pulses," *Phys. Rev. A* **56**, 3870–3878 (1997).
- M. M. Wefers, H. Kawashima, and K. A. Nelson, "Optical control over two-dimensional lattice vibrational trajectories in crystalline quartz," *J. Chem. Phys.* **108**, 10248–10255 (1998).
- D. Kupka, P. Schlup, and R. A. Bartels, "Simplified polarization pulse shaper using a birefringent prism," *Rev. Sci. Instrum.* (to be published).
- M. Plewicki, F. Weise, S. M. Weber, and A. Lindinger, "Phase, amplitude, and polarization shaping with a pulse shaper in a Mach-Zehnder interferometer," *Appl. Opt.* **45**, 8345–8359 (2006).
- G. T. Brixner and G. Gerber, "Femtosecond polarization pulse shaping," *Opt. Lett.* **26**, 557–559 (2001).
- O. Masihzadeh, P. Schlup, and R. A. Bartels, "Complete polarization state control of ultrafast laser pulses with a single linear spatial light modulator," *Opt. Express* **15**, 18025–18032 (2007).
- A. E. Paul, J. A. Bolger, A. L. Smirl, and J. G. Pellegrino, "Time-resolved measurements of the polarization state of four-wave mixing signals from GaAs multiple quantum wells," *J. Opt. Soc. Am. B* **13**, 1016–1025 (1996).
- J. A. Bolger, A. E. Paul, and A. L. Smirl, "Ultrafast ellipsometry of coherent processes and exciton-exciton interactions in quantum wells at negative delays," *Phys. Rev. B* **54**, 11666–11671 (1996).
- W. J. Walecki, D. N. Fittingho, A. L. Smirl, and R. Trebino, "Characterization of the polarization state of weak ultrashort coherent signals by dual-channel spectral interferometry," *Opt. Lett.* **22**, 81–83 (1997).
- J. Piasecki, B. Colombeau, M. Vampouille, C. Froehly, and J. A. Arnaud, "Nouvelle methode de mesure de la reponse impulsionnelle des fibres optiques," *Appl. Opt.* **19**, 3749–3755 (1980).
- B. Hass, "Determination of weak optical pulses in amplitude and phase by measurement of the transient polarization state," *Opt. Lett.* **24**, 543–545 (1999).
- J. José Ferreiro, R. D. L. Fuente, and E. Lago, "Characterization of arbitrarily polarized ultrashort laser pulses by cross-phase modulation," *Opt. Lett.* **26**, 1025–1027 (2001).
- P. Schlup, O. Masihzadeh, L. Xu, R. Trebino, and R. A. Bartel, "Tomographic retrieval of the polarization state of an ultrafast laser pulse," *Opt. Lett.* **33**, 267–269 (2008).
- L. Xu, E. Zeek, and R. Trebino, "Simulations of frequency-resolved optical gating for measuring very complex pulses," *J. Opt. Soc. Am. B* **25**, A70–A80 (2008).
- K. W. Delong, R. Trebino, J. Hunter, and W. E. White, "Frequency-resolved optical gating with the use of second-harmonic generation," *J. Opt. Soc. Am. B* **11**, 2206–2215 (1994).
- D. Keusters, H.-S. Tan, P. O'Shea, E. Zeek, R. Trebino, and W. S. Warren, "Relative-phase ambiguities in measurements of ultrashort pulses with well-separated multiple frequency components," *J. Opt. Soc. Am. B* **20**, 2226–2237 (2003).
- E. Zeek, A. P. Shreenath, P. O'Shea, M. Kimmel, and R. Trebino, "Simultaneous automatic calibration and direction-of-time removal in frequency-resolved optical gating," *Appl. Phys. B* **74**, 265–271 (2002).
- R. Trebino, *Frequency-Resolved Optical Gating: The Measurement of Ultrashort Laser Pulses* (Kluwer Academic, 2002).
- D. N. Fittinghoff, K. W. Delong, R. Trebino, and C. L. Ladera, "Noise sensitivity in frequency-resolved optical-gating measurements of ultrashort pulses," *J. Opt. Soc. Am. B* **12**, 1955–1967 (1995).
- J. C. Lagarias, J. A. Reeds, M. H. Wright, and P. E. Wright, "Convergence properties of the Nelder-Mead simplex method in low dimensions," *SIAM J. Optim.* **9**, 112–147 (1998).